Phys. Status Solidi A, 1–6 (2010) / **DOI** 10.1002/pssa.200982845

physica status solidi a
www.pss-a.com
applications and materials science

Properties of interfaces in amorphous/crystalline silicon heterojunctions

Sara Olibet*[,1], Evelyne Vallat-Sauvain[1], Luc Fesquet[1], Christian Monachon[2], Aïcha Hessler-Wyser[2], Jérôme Damon-Lacoste[1], Stefaan De Wolf[1], and Christophe Ballif[1]

[1] Ecole Polytechnique Fédérale de Lausanne (EPFL), IMT, Photovoltaics and Thin Film Electronics Laboratory, Breguet 2, 2000 Neuchâtel, Switzerland (until 31 December 2008 part of the University of Neuchâtel)
[2] Ecole Polytechnique Fédérale de Lausanne (EPFL), Interdisciplinary Centre for Electron Microscopy (CIME), 1015 Lausanne, Switzerland

Received 1 August 2009, revised 9 November 2009, accepted 13 November 2009
Published online 19 January 2010

PACS 68.35.Ct, 68.37.Lp, 72.20.Jv, 73.20.At, 73.40.Lq, 73.61.Jc

* Corresponding author: e-mail solibet@1366tech.com, Phone: +1-617-5120379

To study recombination at the amorphous/crystalline Si (a-Si:H/c-Si) heterointerface, the amphoteric nature of silicon (Si) dangling bonds is taken into account. Modeling interface recombination measured on various test structures provides insight into the microscopic passivation mechanisms, yielding an excellent interface defect density reduction by intrinsic a-Si:H and tunable field-effect passivation by doped layers. The potential of this model's applicability to recombination at other Si heterointerfaces is demonstrated. Solar cell properties of a-Si:H/c-Si heterojunctions are in good accordance with the microscopic interface properties revealed by modeling, that are, e.g., slight asymmetries in the neutral capture cross-sections and band offsets. The importance of atomically abrupt interfaces and the difficulties to obtain them on pyramidally textured c-Si is studied in combination with transmission electron microscopy.

1 Introduction The efficiency of standard monocrystalline Si (c-Si) solar cells featuring diffused emitters and aluminum back surface fields (BSF) is limited to moderate values by interface recombination. This contrasts with deposition of intrinsic/doped amorphous Si (a-Si:H) layer stacks on c-Si, which effectively passivate the c-Si surfaces and simultaneously form the emitter and BSF, while avoiding the highly recombinative direct contact of metal to c-Si. Such Si heterojunction (HJ) solar cells are fabricated by the company Sanyo [1], resulting with 23% sunlight conversion efficiency in the highest-efficient large area c-Si solar cells [2]. Despite these excellent achievements, the physical understanding of interfaces in a-Si:H/c-Si HJs is limited. In this study, the amphoteric nature of Si dangling bonds (DBs) is considered for modeling a-Si:H/c-Si interface recombination [3], revealing the microscopic nature of this interface passivation scheme. The intuitive interpretation of measured injection-level dependent lifetimes at various a-Si:H/c-Si interfaces is facilitated by means of trajectories on three-dimensional surface recombination rate plots [4]. The use of this amphoteric interface recombination formalism to model recombination at other Si heterointerfaces featuring DBs is demonstrated. For Si HJ solar cell formation, layer stacks with the required properties were identified by modeling. The measured solar cell parameters confirm our modeling results and add up with other researchers findings to a more complete picture of Si HJs. The importance of atomically abrupt interfaces for highest passivation quality was confirmed in this study by combining lifetime measurements with transmission electron microscopy (TEM), quantifying the detrimental effect of epitaxial interfaces, that could finally also be suppressed in textured Si HJs.

2 Experimental Hydrogenated amorphous and microcrystalline silicon (a-Si:H and μc-Si:H) layers were grown by very high frequency plasma enhanced chemical vapor deposition (VHF-PECVD) in a single chamber deposition system. SiH_4, H_2, PH_3, and trimethylboron (TMB: $B(CH_3)_3$) were used as precursor gases to grow intrinsic (*i*) a-Si:H and doped μc-Si:H layers on c-Si wafers.

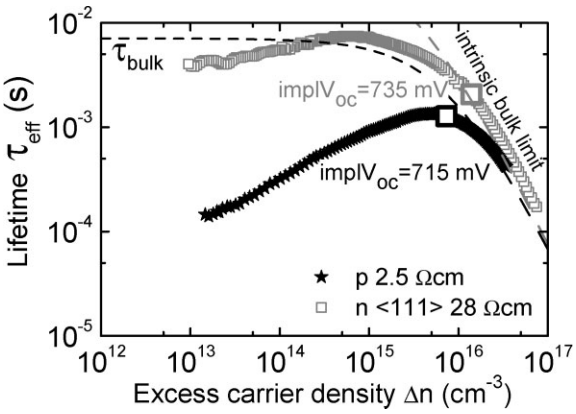

Figure 1 Effective charge carrier lifetime τ_{eff} as a function of the excess carrier density Δn measured by the photoconductance technique.

The properties of a-Si:H/c-Si heterointerfaces were studied by means of the photoconductance technique measuring the effective charge carrier lifetime τ_{eff} (s) as a function of the excess carrier density Δn (cm^{-3}) [5], see Fig. 1. Using the highest quality of c-Si wafers, heterostructures are dominated by their interface properties quantified by the effective surface recombination velocity S_{eff} (cm/s), accessible from τ_{eff} by

$$S_{eff} = \frac{(\tau_{eff}^{-1} - \tau_{b,intr}^{-1})W}{2}, \quad (1)$$

where symmetrical surface passivation is assumed, W is the wafer thickness and intrinsic bulk c-Si recombination ($\tau_{b,intr}$) only dominates at high Δn [6], see again Fig. 1. The absolute lifetime values as well as their injection-level dependencies are given by the specific interface passivation mechanisms. From such $\tau_{eff}(\Delta n)$ plots one can additionally extract the very valuable information of the 1-sun illumination-level open-circuit voltage (V_{oc}) that a solar cell with these interface recombination properties, and based on this wafer would have, called the implied V_{oc} (implV_{oc}), see again Fig. 1 [5].

3 Modeling The surface recombination rate U (cm^2/s) is related to the experimentally accessible S_{eff} by

$$U = S_{eff}\Delta n, \quad (2)$$

where $\Delta n = \Delta p$ is the bulk excess carrier density generated, e.g., by illumination. Recombination through defect levels in semiconductors is usually described by the Shockley–Read–Hall (SRH) theory, where the single trap level surface recombination rate U_{SRH} is given by

$$U_{SRH} = \frac{n_s p_s}{n_s/\sigma_p + p_s/\sigma_n} v_{th} N_s. \quad (3)$$

Without additional surface charges, the surface carrier densities n_s, p_s equal the bulk carrier densities $n_b = n_0 + \Delta n$ and $p_b = p_0 + \Delta n$, where n_0, p_0 are the thermal equilibrium

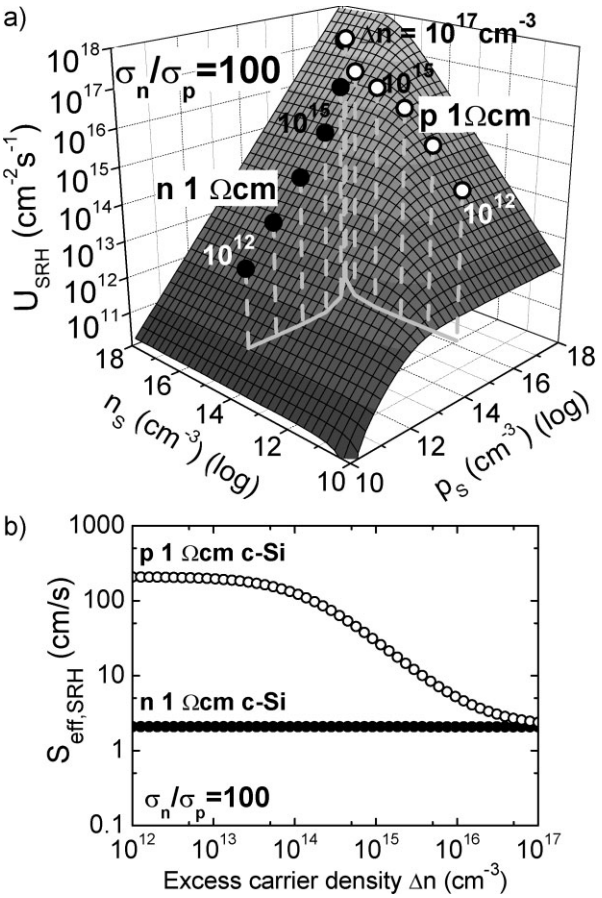

Figure 2 Impact of the wafer doping for a given capture cross-section ratio σ_n/σ_p on (a) the surface recombination rate $U_{SRH}(n_s, p_s)$ and (b) the surface recombination velocity $S_{eff,SRH}(\Delta n)$.

charge carrier densities. σ_n and σ_p (cm^2) are the capture cross-sections of electrons and holes, v_{th} (cm/s) is the thermal velocity of the charge carriers, and N_s (cm^{-2}) is the surface defect density. Figure 2a visualizes $U_{SRH}(n_s, p_s)$ (Eq. 3) for the capture cross-section ratio generally assumed to model SiO_2/c-Si interface recombination, i.e., $\sigma_n/\sigma_p = 100$ [7]. In our experiments, the carrier density Δn, thus n_s and p_s vary and U varies accordingly, as shown in Fig. 2a by means of the trajectories for 1 Ω cm n- and p-type c-Si. Figure 2b shows the corresponding $S_{eff,SRH}(\Delta n)$ plots (Eq. 2). With the capture cross-section asymmetry of $\sigma_n > \sigma_p$, surface recombination at the SiO_2/p c-Si interface is thus higher than at the SiO_2/n c-Si interface.

A surface charge density Q_s (cm^{-2}) results in a surface band bending ψ_s (V) and thus the surface carrier densities differ from the ones in the bulk: $n_s = n_b \exp(+q\Psi_s/kT)$ and $p_s = p_b \exp(-q\Psi_s/kT)$. Figure 3 shows the effect of a positive surface charge, as e.g., reported at the SiN_x/c-Si interface, on the trajectories on the $U_{SRH}(n_s, p_s)$ plot for equal capture cross-sections and 1 Ω cm n- and p-type c-Si. While repelling the minority holes from the n-type c-Si surface reduces interface recombination, attracting the

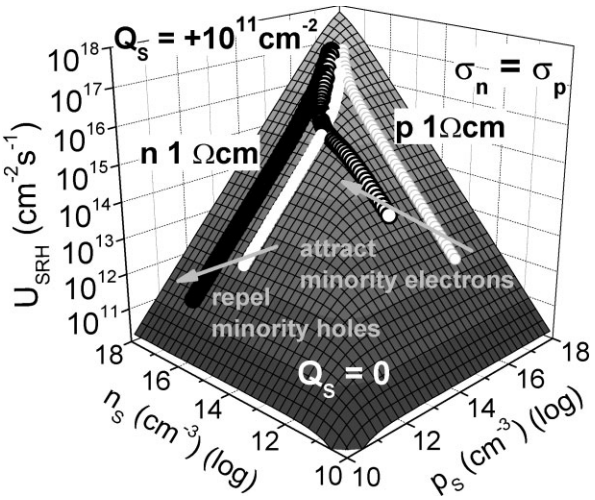

Figure 3 Impact of the surface charge density Q_s and the wafer doping on the trajectories on the surface recombination rate plot $U_{SRH}(n_s, p_s)$.

minority electrons to the p-type c-Si surface increases the surface recombination rate, as compared to the flatband case.

The standard SRH surface recombination model is based on interface traps having two possible charge states. Because the bare c-Si surface as well as a-Si:H feature DBs, we propose to model heterostructure interface recombination by amphoteric defects, i.e., DBs having three possible charge states. For this, we extended a model previously established for bulk a-Si:H recombination assuming one single recombination level with three charge conditions [8] to the c-Si surface, resulting in the surface DB recombination rate U_{DB}

$$U_{DB} = \frac{n_s\sigma_n^0 + p_s\sigma_p^0}{(p_s/n_s)(\sigma_p^0/\sigma_n^+) + 1 + (n_s/p_s)(\sigma_n^0/\sigma_p^-)} v_{th} N_s, \tag{4}$$

where σ_n^0, σ_p^0 are the capture cross-sections of the neutral states and σ_n^+, σ_p^- are the capture cross-sections of the charged states. Note that to find Eq. (4) the illumination level must be high enough to neglect emission from DB states [8]. Best fits of our experimental data are obtained with $\sigma_n^0/\sigma_p^0 = 1/20$ and $\sigma_n^+/\sigma_n^0 = \sigma_p^-/\sigma_p^0 = 500$. The same capture cross-section hierarchy of $\sigma_n^0 < \sigma_p^0 < \sigma_n^+ < \sigma_p^-$ is found in amorphous semiconductors by Street [9], although much less pronounced. The surface plot of $U_{DB}(n_s, p_s)$, shown in Fig. 4, has a local minimum whose position is given mainly by the neutral capture cross-section ratio. Within its width determined by the charged to neutral capture cross-section ratios, recombination is dominated by majority carriers and thus opposite to the common SRH recombination. Comparing the Δn-dependent trajectories on the $U_{DB}(n_s, p_s)$ plot in Fig. 4 to the ones similar to SiO_2- and SiN_x-passivated c-Si in Figs. 2 and 3, shows that a-Si:H passivation is more symmetrical as far as surface passivation of both wafer doping types is concerned. Fits to measured $\tau_{eff}(\Delta n)$ plots are obtained by combining

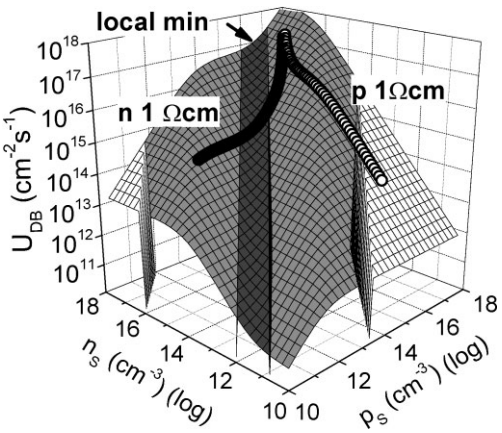

Figure 4 Surface recombination rate $U_{DB}(n_s, p_s)$ based on the amphoteric nature of c-Si surface dangling bonds, including examples of Δn-dependent trajectories.

Eq. (1), (2), and (4)

$$\tau_{eff}^{-1} = \tau_b^{-1} + \left(\frac{2}{W}\right)\left(\frac{1}{\Delta n}\right) \times U_{DB}(\Delta n; n_0, p_0; Q_s; N_s; \sigma_p^0, \sigma_n^0/\sigma_p^0, \sigma^{+,-}/\sigma^0). \tag{5}$$

4 Results

4.1 *i* a-Si:H passivation of various c-Si Figure 5 shows by symbols the measured injection-level dependent lifetimes of *i* a-Si:H passivating variously doped flat c-Si, implying excellent open-circuit voltages implV_{oc} over 700 mV throughout, see legend. Thus, the simple low temperature a-Si:H passivation scheme compares favorably to best performing SiO_2 and SiN_x layers [6, 10]. Best a-Si:H/c-Si interface passivation with surface recombination

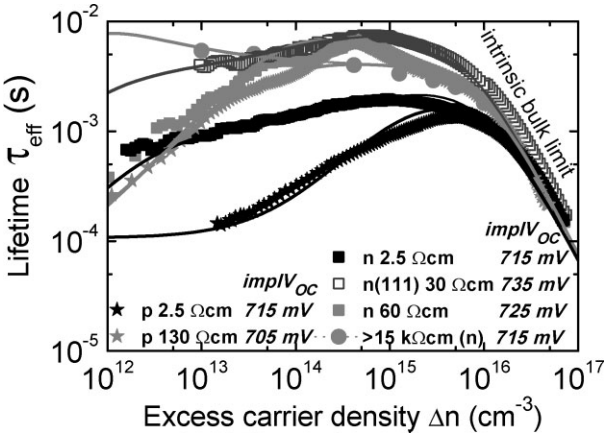

Figure 5 Lifetimes τ_{eff} of *i* a-Si:H passivating differently doped flat c-Si. Symbols are measurements and lines are fits with our amphoteric interface recombination model using the parameters listed in Table 1.

Table 1 Model parameter couples interface dangling bond density N_s/charge density Q_s, giving best accordance between the measured and calculated $\tau_{eff}(\Delta n)$ plots in Fig. 5. $\sigma_p^0 = 10^{-16}\,cm^2$ is assumed.

i a-Si:H on	N_s ($10^9\,cm^{-2}$)	Q_s ($10^{10}\,cm^{-2}$)
n 2.5 Ω cm	1.0	−2.2
n (111) 30 Ω cm	0.45	−0.5
n 60 Ω cm	1.6	+1.1
>15 kΩ cm (n)	1.6	+0.1
p 2.5 Ω cm	1.4	+1.8
p 130 Ω cm	3	+0.5

velocities S_{eff} down to 1 cm/s were measured on (111) crystal oriented c-Si, likely related to the possibility of perfect monohydride hydrogen termination of such (111) surfaces [11] despite their higher DB density. This is opposite to SiO_2 and SiN_x where the passivation of (111) oriented c-Si is inferior to the one of (100) oriented c-Si [12]. Concerning the application of passivation in the industrially relevant textured monocrystalline Si solar cells featuring (111) oriented pyramidal facets, this is an important finding. Figure 5 includes by lines fits to the experimental curves obtained with our amphoteric interface recombination model. The extracted values of the interface DB density N_s and the charge density Q_s for the different wafers are listed in Table 1. Q_s is the DB charge within the passivating a-Si:H layer inducing the image charge Q_{Si} in the c-Si surface [4]. In the present case of intrinsic a-Si:H passivating variously doped c-Si, the interface DB charge is determined by the wafer doping type and level, by band offset asymmetries and the lightly n-type doped character of nominally intrinsic a-Si:H. For example, best fits obtained with negative charge in *i* a-Si:H at the interface to clearly n-type doped c-Si and positive charge in *i* a-Si:H to p-type doped c-Si confirm the amphoteric nature of a-Si:H/c-Si interface defects.

4.2 a-Si:H/c-Si field-effect passivation Unlike SiN_x (and less pronounced also SiO_2) featuring a positive interface charge when grown on c-Si, in the case of a-Si:H, field-effect passivation of both charge types can be

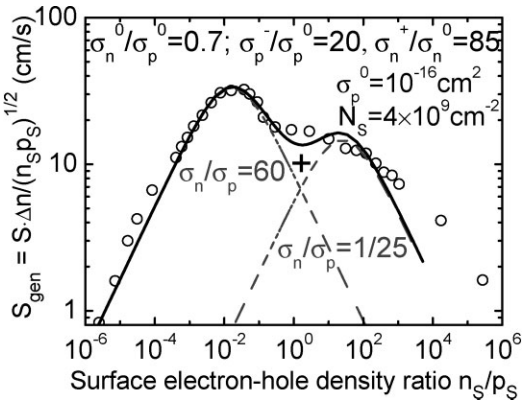

Figure 7 SiO_2/c-Si interface recombination as a function of n_s/p_s measured by Yablonovitch et al. [14]. Fits with two standard SRH interface states of different capture cross-section ratios (dashed lines, adding up) and fits with amphoteric interface states (solid line) coincide.

controlled by varying the average state of charge on the interface DBs, e.g., by an overlaying doped μc-Si:H layer. The *i* a-Si:H buffer layer in such intrinsic/doped layer stacks ensures a low interface defect density N_s. Figure 6 shows experimental $\tau_{eff}(\Delta n)$ plots of intrinsic/doped layer stacks such as used for silicon HJ solar cell formation on 2.5 Ω cm n-type (a) and p-type (b) c-Si together with their fits. The subsequent representation in terms of trajectories over surface recombination rate plots in Fig. 6c allows for an easier, more intuitive interpretation of these $\tau_{eff}(\Delta n)$ plots. The $U_{DB}(n_s, p_s)$ plot in Fig. 6c thus illustrates that the measured lower lifetimes at low injection levels on p-type (open symbols) than on n-type (full symbols) c-Si result from the slight neutral capture cross-section asymmetry, leading in general to higher recombination when $p_s > n_s$.

4.3 Modeling of SiO_2/c-Si interface recombination by amphoteric states The identification of SiO_2/c-Si interface defects as DBs [13] allows for a broader application of our amphoteric interface recombination formalism. Yablonovitch et al. [14] measured SiO_2/c-Si interface recombination as a function of n_s/p_s, see symbols in Fig. 7, and

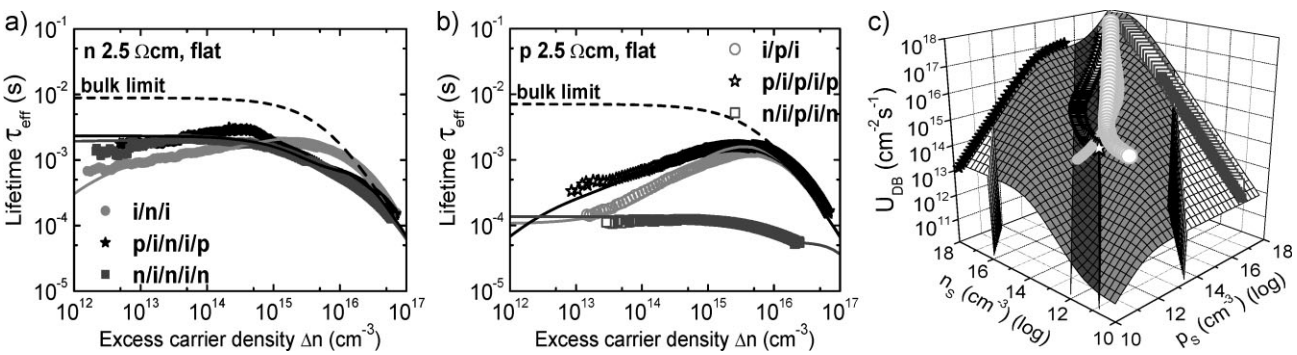

Figure 6 Additional field-effect passivation by internally polarizing *i* a-Si:H layers with an overlaying doped μc-Si:H layer on 2.5 Ω cm n-type (a) and p-type (b) c-Si. Symbols are measured $\tau_{eff}(\Delta n)$ plots and lines are their fits, also represented in terms of trajectories over surface recombination rate plots to facilitate their intuitive interpretation (c).

fitted their data by adding up the SRH recombination due to two individual interface states of different capture cross-section ratios. The dashed lines in Fig. 7 show such a fit with a dominant defect of $\sigma_n/\sigma_p = 60$ and a lesser one of $\sigma_n/\sigma_p = 1/25$. Our modeling of the same data with amphoteric interface DBs represented by the bold line in Fig. 7 yields exactly the same fit, but with a physical meaning attributed to the fit parameters, that is larger charged than neutral capture cross-sections.

4.4 a-Si:H/c-Si heterojunctions a-Si:H/c-Si HJ solar cells must feature simultaneously lowest interface defect densities for highest open-circuit voltages (V_{oc}) and highest doped layers for highest fill factors (FF), with the thinnest layers possible, to allow for current extraction. Thus, the modeling assisted interpretation of measured lifetime curves permits the development of suitable layer stacks for Si HJ solar cell formation, which were found to consist of very thin *i* a-Si:H layers providing excellent interface passivation to c-Si, followed by under high H_2-dilution grown highest doped μc-Si:H layers ensuring best carrier extraction from the a-Si:H/c-Si HJ. A 19.1% efficient (4.5 mm^2) surfaced Si HJ solar cell was reached on flat n-type c-Si with [V_{oc} (mV), FF (%), J_{sc} (mA/cm^2), η (%)] = [680, 82, 34, 19.1], where J_{sc} is the short-circuit current density and η the efficiency. With a slightly thicker *i*-layer, high V_{oc} Si HJs were achieved with n-wafer = [705, 78, 32, 17.6] and p-wafer = [690, 74, 32, 16.3]. The slight neutral capture cross-section asymmetry and the band offset asymmetry, see Fig. 6 and Table 1 including related comments, give an explanation for the poorer performance of Si HJs based on p-wafers. The best V_{oc}s of 730 mV were obtained on (111) oriented c-Si, as predicted by *i* a-Si:H passivation, see Fig. 5. We relate the poor FFs of typically 50% of such cells partially to the lower doping level of this wafer (30 Ω cm) making the required tunneling transport across the ITO(n)/p μc-Si:H/*i* a-Si:H/n c-Si interface even more challenging [15].

4.5 Atomic a-Si:H/c-Si interfaces From the crystallographic point of view, abrupt interfaces are the key to low interface recombination. As first observed by Wang et al. [16] interface recombination increases when epitaxized interfaces occur. For example, under the same process conditions grown highly H_2 diluted *i* a-Si:H layer leads to best interface passivation on flat (111) oriented c-Si, but to epitaxized (100) oriented c-Si interfaces as observed by high resolution transmission electron microscopy (HR-TEM). Presumably the (111) c-Si surface benefits from an increased monohydride hydrogen passivation [11] while the (100) c-Si surface suffers from an epitaxial interface of low quality and an increased a-Si:H/c-Si interface area [4]. The resulting increase in interface recombination by a factor of 40 corresponds, e.g., to an implV_{oc} decrease from 710 down to 600 mV. On pyramidally textured c-Si featuring (111) facets, local epitaxial growth in the pyramid grooves, presumably resulting from stress, increases interface recombination by a factor of 4 when featuring large pyramids, reducing implV_{oc}, e.g., from 720 to 675 mV. However, if epitaxial growth is suppressed, implV_{oc}s even higher than on flat (100) c-Si were reached despite the increased textured interface area, because of the superior passivation of the (111) oriented pyramid facets over the flat (100) oriented c-Si.

On the Si HJ solar cell level, HR-TEM micrographs confirm the abrupt nature of the interfaces in our best performing flat Si HJ solar cells consisting of c-Si/*i* a-Si:H/doped μc-Si:H layers, see Fig. 8a. On pyramidally textured c-Si, abrupt facet interfaces but epitaxized texture grooves, see Fig. 8b, related to the growth of only thin *i* a-Si:H layers followed by the deposition of an overlaying doped μc-Si:H layer grown under very high H_2 dilution, lead to lowered V_{oc}s of 660 mV on n-type doped c-Si. Reducing not only the groove density per projected surface area by using large, regular pyramidally textured c-Si, but blunting additionally the sharp pyramidal grooves, could reduce the amount of epitaxized a-Si:H/c-Si interfaces. Thus, textured Si HJ solar

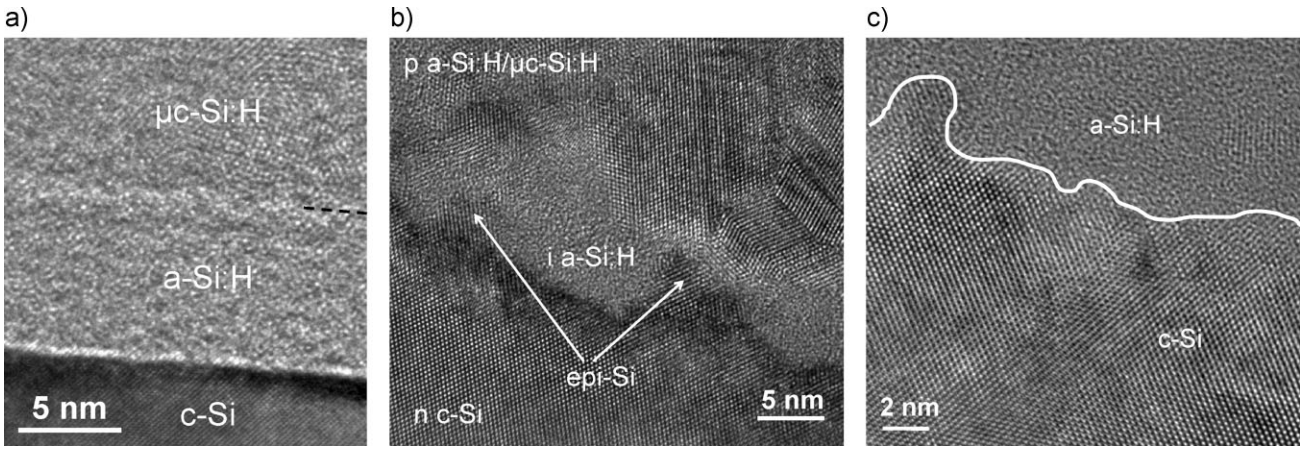

Figure 8 HR-TEM micrographs showing (a) abrupt flat crystallographic c-Si/a-Si:H/μc-Si:H interfaces of Si HJ solar cells, (b) an epitaxially connected *i* a-Si:H interface passivation layer in the pyramidal groove of a textured Si HJ solar cell, and (c) a rough a-Si:H/c-Si interface, also of a textured Si HJ solar cell.

cells with V_{oc}s up to 705 mV were reached. The remaining FF limitation of 70% observed on these cells is possibly related to the rough nature of the heterointerface resulting from the wet-chemical etching of c-Si, see Fig. 8c. Angermann et al. [17] indeed report major FF improvements by smoothing such nanoroughnesses.

5 Conclusions The growth of intrinsic a-Si:H on c-Si minimizes interface recombination as effectively as SiO_2 and SiN_x, but with more symmetry as far as the passivation of different doping types and levels is concerned. In this study, the specific properties of Si DBs to possess three charge states are successfully taken into account for modeling recombination measured at various a-Si:H/c-Si interfaces. The extraction of interface charge density values from modeling charge carrier lifetime measurements of *i* a-Si:H grown on differently doped c-Si confirms the amphoteric interface nature. Additionally, in contrast to SiO_2 and SiN_x, a-Si:H passivation of the solar cell industry more relevant (111) oriented c-Si surfaces (pyramidal facets of textured (100) c-Si) is superior over (100) c-Si. The contribution of field-effect passivation can be tuned by an overlaying doped μc-Si:H layer such as used in Si HJ solar cell formation. The representation of lifetime curves in terms of trajectories over three-dimensional surface recombination rate plots facilitates the intuitive interpretation. The identified slight asymmetry in the electron and hole capture cross-sections on neutral defects results together with the band offset asymmetry in the measured lower performance of p- as compared to n-type c-Si based HJ solar cells. The presented amphoteric interface recombination model is not limited to the a-Si:H/c-Si interface but is successfully applied to the SiO_2/c-Si interface and could potentially be used to model all Si heterointerface recombination featuring DBs. The importance of the atomically abrupt nature of a-Si:H/c-Si interfaces is quantified by comparison of interface recombination measurements and HR-TEM micrographs. On textured c-Si, although the (111) crystal oriented c-Si pyramid facets feature lowest interface recombination, local epitaxy in sharp pyramidal grooves lead to increased interface recombination that limits the efficiency of textured solar cells. By suppressing epitaxial growth in pyramid grooves, textured solar cell V_{oc}s could be improved by the same amount as the one implied by lifetime measurements on *i* a-Si:H/c-Si test structures featuring epitaxized pyramid grooves, proving once more the usefulness of lifetime measurements on simple test structures for solar cell development.

Acknowledgements This work was supported by the Swiss National Science Foundation (Grant SNSF 200020-116630), by the University of Neuchâtel, and by the Axpo Holding AG, Switzerland in the frame of the Axpo Naturstrom Fond.

References

[1] Y. Tsunomura, Y. Yoshimine, M. Taguchi, T. Baba, T. Kinoshita, H. Kanno, H. Sakata, E. Maruyama, and M. Tanaka, Sol. Energy Mater. Sol. Cells **93**, 670–673 (2009).
[2] M. Green, K. Emery, Y. Hishikawa, and W. Warta, Prog. Photovolt., Res. Appl. **17**, 320–326 (2009).
[3] S. Olibet, E. Vallat-Sauvain, and C. Ballif, Phys. Rev. B **76**, 035326 (2007).
[4] S. Olibet, Interface properties of amorphous/crystalline silicon heterojunctions (Südwestdeutscher Verlag für Hochschulschriften, Saarbrücken, 2009).
[5] R. Sinton and A. Cuevas, Appl. Phys. Lett. **69**, 2510–2512 (1996).
[6] M. Kerr and A. Cuevas, Semicond. Sci. Technol. **17**, 166–172 (2002).
[7] S. Glunz, D. Biro, S. Rein, and W. Warta, J. Appl. Phys. **86**, 683–691 (1999).
[8] J. Hubin, A. Shah, and E. Sauvain, Philos. Mag. Lett. **66**, 115–125 (1992).
[9] R. Street, Philos. Mag. B **49**, 15–20 (1984).
[10] M. Kerr and A. Cuevas, Semicond. Sci. Technol. **17**, 35–38 (2002).
[11] G. S. Higashi, Y. J. Chabal, G. W. Trucks, and K. Raghavachari, Appl. Phys. Lett. **56**, 656–658 (1990).
[12] F. Schuurmans, A. Schönecker, J. Eikelboom, and W. Sinke, Proceedings of the 25th IEEE Photovoltaic Specialists Conference, IEEE, New York, 1996, pp. 485–488.
[13] D. Biegelsen, N. Johnson, M. Stutzmann, E. Poindexter, and P. Caplan, Appl. Surf. Sci. **22/23**, 879–890 (1985).
[14] E. Yablonovitch, R. Swanson, W. Eades, and B. Weinberger, Appl. Phys. Lett. **48**, 245–247 (1986).
[15] A. Kanevce and W. K. Metzger, J. Appl. Phys. **105**, 094507 (2009).
[16] T. Wang, E. Iwaniczko, M. Page, D. Levi, Y. Yan, V. Yelundur, H. Branz, A. Rohatgi, and Q. Wang, Proceedings of the 31st IEEE Photovoltaic Specialists Conference, IEEE, New York, 2005, pp. 955–958.
[17] H. Angermann, E. Conrad, L. Korte, J. Rappich, T. Schulze, and M. Schmidt, Mater. Sci. Eng. B **159–160**, 219–223 (2009).

